This manuscript has been accepted for presentation in the 20th IEEE International Symposium on Biomedical Imaging, Cartagena de Indias, Colombia, April 18-21, 2023.

Prostate Capsule Segmentation in Micro-Ultrasound Images Using Deep Neural Networks

[1]Wenbin Guo, [2]Wayne Brisbane, [2]Rani Ashouri, [2]Brianna Nguyen, [1]Angelos Barmpoutis

[1]Digital Worlds Institute, University of Florida, Gainesville, FL
[2]Department of Urology, University of Florida, Gainesville, FL

ABSTRACT

Prostate cancer is the most common internal malignancy among males. Micro-Ultrasound is a promising imaging modality for cancer identification and computer-assisted visualization. Identifying the prostate capsule area is essential in active surveillance monitoring and treatment planning. In this paper, we present a pilot study that assesses prostate capsule segmentation using the U-Net deep neural network framework. To the best of our knowledge, this is the first study on prostate capsule segmentation in Micro-Ultrasound images. For our study, we collected multi-frame volumes of Micro-Ultrasound images, and then expert prostate cancer surgeons annotated the capsule border manually. The lack of clear boundaries and variation of shapes between patients make the task challenging, especially for novice Micro-Ultrasound operators. In total 2099 images were collected from 8 subjects, 1296 of which were manually annotated and were split into a training set (1008), a validation set (112), and a test set from a different subject (176). The performance of the model was evaluated by calculating the Intersection over Union (IoU) between the manually annotated area of the capsule and the segmentation mask computed from the trained deep neural network. The results demonstrate high IoU values for the training set (95.05%), the validation set (93.18%) and the test set from a separate subject (85.14%). In 10-fold cross-validation, IoU was 94.25%, and accuracy was 99%, validating the robustness of the model. Our pilot study demonstrates that deep neural networks can produce reliable segmentation of the prostate capsule in Micro-Ultrasound images and pave the road for the segmentation of other anatomical structures within the capsule, which will be the subject of our future studies.

Index Terms— U-Net, deep neural networks, prostate capsule segmentation, prostate cancer, Micro-Ultrasound

1. INTRODUCTION

Prostate cancer is the most common solid malignancy among American men, with 268,000 projected diagnoses in 2022 [1]. Conventional ultrasound is unable to differentiate cancer from benign tissue [2]. Over the last decade, two significant advances in imaging have improved the visualization of prostate cancer. First, the introduction of Magnetic Resonance Imaging (MRI) led to an increase in the accuracy of cancer diagnosis [3], [4]. Second, the use of Micro-Ultrasound further improved the visualization of cancer compared to MRI [5]. Prostate MRI enables clinicians to identify prostate cancer and suspicious target areas for biopsy utilizing MRI/ultrasound fusion. Use of MRI to aid prostate cancer diagnosis is now the standard of care. However, the time, cost, and limited availability of scanners are amplified if MRI is used for in-bore biopsy. The accuracy of Micro-Ultrasound for prostate biopsy has demonstrated better performance than MRI guidance in the detection of prostate cancer.

Studies compared Micro-Ultrasound imaging with MRI and conventional ultrasound for visualizing prostate cancer in active surveillance [6], [7]. High-resolution Micro-Ultrasound was demonstrated to be sensitive to significant prostate cancer and effective for biopsy targeting. Micro-ultrasound was performed in real-time during the biopsy procedure and improved imaging resolution over conventional ultrasound imaging, thereby enabling targeting of these biopsies. Micro-Ultrasound increased the detection probability of clinically significant cancer and decreased the disease risk early.

Manual segmentation is still the most common way to accurately annotate the prostate capsule area. However, manual prostate segmentation is time-consuming and subject to surgeons' experience level. Prostates have a wide range of shapes and sizes, and surgeons need to be trained to annotate the prostate area on grayscale ultrasound images. The ambiguity of its boundaries makes it very hard to differentiate the capsule from the surrounding area with the intraprostatic area.

While several algorithms have been published for automated prostate capsule annotation in MRI and conventional ultrasound [8]–[12], no algorithms have been tested for Micro-Ultrasound. Additionally, Micro-Ultrasound has several unique features making algorithm design challenging: inconsistent image spacing, non-uniform voxel orientation, sagittal image acquisition, and pixel resolution degradation distant from the transducer. Therefore, our aim is to develop a solution for automated prostate capsule segmentation in Micro-Ultrasound images that will assist

prostate cancer surgeons during the biopsy procedure by providing real-time annotation.

Our contributions in this paper are twofold: a) we present a method for prostate capsule segmentation in Micro-Ultrasound images using a modified U-Net-based deep neural network framework, and b) we present a pilot study for assessing the segmentation results using a dataset of 1296 manually annotated Micro-Ultrasound images from eight subjects, including one separate subject for the test set. The results demonstrate reliable segmentation performance measured by accuracy as well the intersection over union metric. Additionally, 10-fold cross-validation demonstrated the robustness of our model. To the best of our knowledge, this is the first study on prostate capsule segmentation in Micro-Ultrasound images.

2. METHOD

2.1. Dataset Acquisition and Preprocessing

The Micro-Ultrasound images that were used in this study were obtained as part of a clinical evaluation for patients with suspected prostate cancer. Images were acquired in a standard transrectal fashion utilizing an EV-29L probe imaging at 29 MHz achieving a resolution of 70 microns [13]. The probe was rotated in a clockwise fashion to acquire serial images from the patient's right lateral prostate edge through the urethra to the left lateral edge. The prostate capsule was annotated by an expert prostate cancer surgeon (co-author Wayne Brisbane) and utilized for training and validation. This analysis was approved by the University of Florida Institutional Review Board (IRB202200785).

In total, 2099 Micro-Ultrasound images were collected from 8 subjects, 1296 of which were annotated, by manually identifying the border of the prostate capsule.

Table 1. Dataset.

Dataset	Images	Annotated Images
UCLA001	166	163
UCLA002	278	91
UCLA003	253	233
UCLA004	202	37
UF001	300	184
UF002	300	202
UF003	300	210
UF004	300	176
Total	**2099**	**1296**

The obtained images were in DICOM (Digital Imaging and Communications in Medicine) format, and were pre-processed in Python using the pydicom and OpenCV APIs in order to extract the grayscale Micro-Ultrasound images and convert the manual annotation from point sequences into binary masks of same resolution as the Micro-Ultrasound images. The primary key Instance UID of the original DICOM images was used as a unique identifier of the extracted images and masks for easy retrieval and referencing.

Two dictionaries were created using these unique identifiers. One is the raw image dictionary (X), and another is the mask dictionary (Y) which were used in our deep neural network model training. X was the feature, and Y was the target value in the training and prediction.

2.2. U-Net Model Design

UNet enables precise localization by predicting the image pixel by pixel. Studies have shown that the UNet was strong enough to make good predictions based on very few training images and achieve high performance in segmentation [14]. We modified the UNet model based on femoral nerve block region segmentation on ultrasound images [15]. Table 2 shows the architecture of the UNet model with 9 unit levels consisting of the contracting path, bottleneck, and expanding path, with two convolutional layers in each level.

Table 2. Modified U-Net architecture.

	Unit Level	Layers	Output
Input			256x256x1
Contracting	Level 1	Conv 1	256x256x8
		Conv 2	256x256x8
	Level 2	Conv 3	128x128x16
		Conv 4	128x128x16
	Level 3	Conv 5	64x64x32
		Conv 6	64x64x32
	Level 4	Conv 7	32x32x64
		Conv 8	32x32x64
Bottleneck	Level 5	Conv 9	16x16x128
		Conv 10	16x16x128
Expanding	Level 6	Conv 11	32x32x64
		Conv 12	32x32x64
	Level 7	Conv 13	64x64x32
		Conv 14	64x64x32
	Level 8	Conv 15	128x128x16
		Conv 16	128x128x16
	Level 9	Conv 17	256x256x8
		Conv 18	256x256x8
Output			256x256x1

First, we resize all raw grayscale images to 256 × 256 pixels and normalize their intensity values from [0, 255] to the range [0, 1]. The contracting path follows the block diagram in Figure 1.

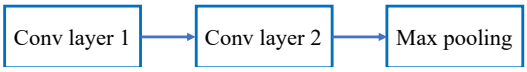

Fig. 1. Contracting path block diagram

In this architecture, each contracting level consists of two convolutional layers followed by a rectified linear unit

(ReLU) function, and the number of channels changes from 1 to 128, as the convolution process increases the depth of the image. The max pooling process reduces the size of the image by half, and padding is used to keep the size of the images the same. This process is repeated four times.

Second, at the bottleneck level, the UNet model still has two convolutional layers followed by ReLU but with no max pooling layers. Adding one dropout layer with 10% between convolutional layers can reduce the overfitting in the training. The images are resized to 16x16x128.

Third, in the expanding path, the images are upsized to their original input size, following the steps shown in Figure 2.

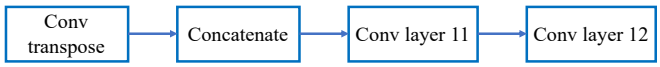

Fig. 2. Expanding path block diagram

Transposed convolution is an upsampling technology to double the size of image by adding padding to the original image followed by a 2x2 convolution. The image is upsized from 16x16x128 to 32x32x64. Next, this image is concatenated with the corresponding size image from the contracting path to make an image of size 32x32x128, which improves the precision of the prediction. After that, two convolution layers followed by ReLU are added and this process is repeated four times.

The last step is to reshape the output image to match our input image size with a final 1x1 convolution layer.

For assessing image segmentation results, the Dice similarity coefficient and intersection over union (IoU) have been widely used as metrics in training deep neural networks. In our preliminary tests we found similar performance between the Dice score and IoU score with a negligible difference (1-2%). Therefore, our modified UNet model was compiled with adam optimizer, binary cross entropy loss function and IoU score, calculated as follows:

$$IoU = Area\ of\ Overlap / Area\ of\ Union \quad (1)$$

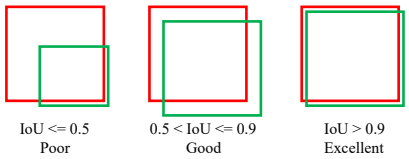

Fig. 3. IoU score threshold

In our network training, no early stopping was added, the epochs were 100, the batch size was 32, and the validation split was 10%. Based on the threshold of IoU score in Figure 3, an IoU > 0.5 is considered an effective segmentation. According to this threshold, segmentation accuracy is defined as follows:

$$Accuracy = \frac{N.of\ images\ with\ (IoU>0.5)}{Total\ number\ of\ images} \quad (2)$$

3. RESULTS

The modified UNet model was developed and tested in the UF High-Performance Computing Facility (HiPerGator). The results of IoU score and loss after 100 epochs as shown in Figure 4. The training set (1008 images from 7 subjects) had IoU 95.05%, and the validation set (112 images from the same 7 subjects) had IoU 93.18%.

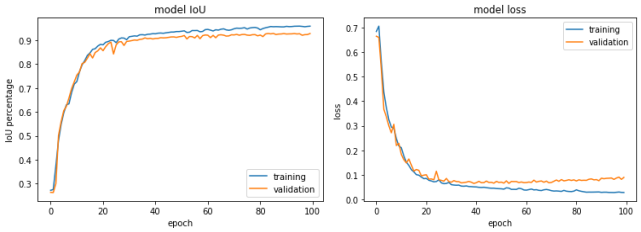

Fig. 4. Model IoU (Left) and Loss (Right) in training and validation with 100 epochs

Our test set consisted of 176 images from a separate subject in order to eliminate the within-group effect on the test accuracy. Because of the expected differences in shape and size of the prostate capsule of the subject in our test set, the IoU was 85.14%, which was slightly less compared to the IoU in the training and validation sets. However, even in this case the IoU was still greater than 50%, which is considered an effective segmentation result. Figure 5 shows the IoU in the three different sets.

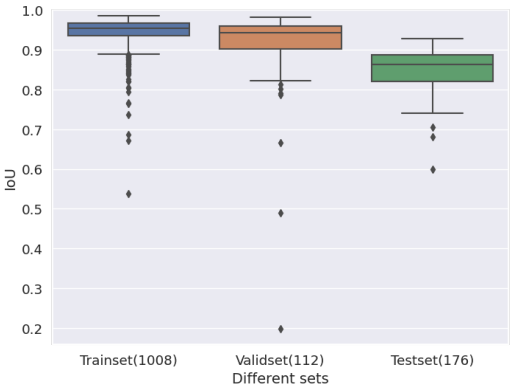

Fig. 5. IoU in three different sets

The prediction duration for each image was 0.048 second using the GPU NVIDIA GeForce RTX 2080 Ti, demonstrating that the model can be used for the real-time prostate segementation. The source code is available at: https://github.com/digitalworlds/ProstateSegmentation.

Figure 6 shows two examples of annotation from the UCLA dataset (Left) and the UF dataset (Right). The first row shows the original Micro-Ultrasound images from the two datasets. The second row shows the manually annotated "ground truth" masks of the prostate capsule. The third row presents the predicted masks. In the left image the calculated IoU is 96.78%, and in the right image IoU is 94.46%.

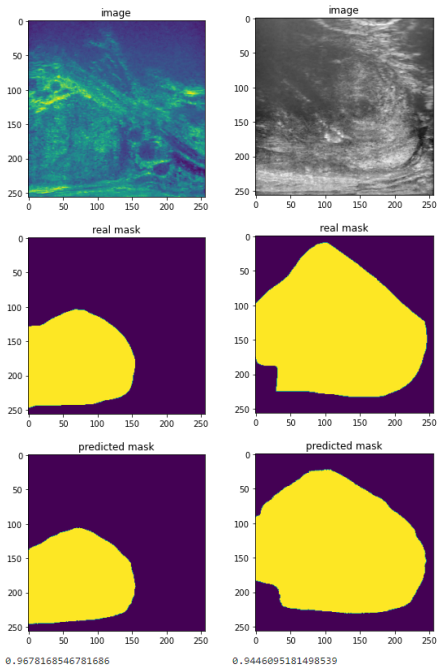

Fig. 6. Visual comparison of the segmentation results on two subjects (Left:UCLA dataset and right:UF dataset).

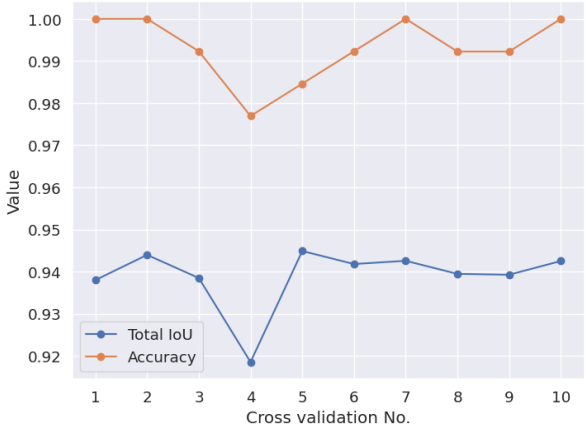

Fig. 7. 10-fold cross-validation.

4. DISCUSSION

As shown in Figure 5, all three data sets (training, validation, and testing) demonstrated high IoU values, well above the 0.5 lower limit. As expected, the IoU values from the test set were less than those in the training and validation sets, primarily because of the expected differences in the anatomy of the capsule in the test subject. By comparing the manual annotations and the calculated segmentations in Figure 6, it seems that the manual annotations have more sharp corners and features compared to the segmentation results which tend to be more round. Accuracy depended on the manually annotated datasets, which could be biased. Therefore, we used 10-fold cross-validation, as shown in Figure 7, using all the subjects from UF and UCLA datasets, and the IoU was above 0.9, which demonstrates that our modified UNet algorithm is suitable for segmenting the prostate capsule. Finally, Figure 8 shows the segmentation results of our method in three different Micro-Ultrasound frames from the same subject that correspond to different parts of the capsule.

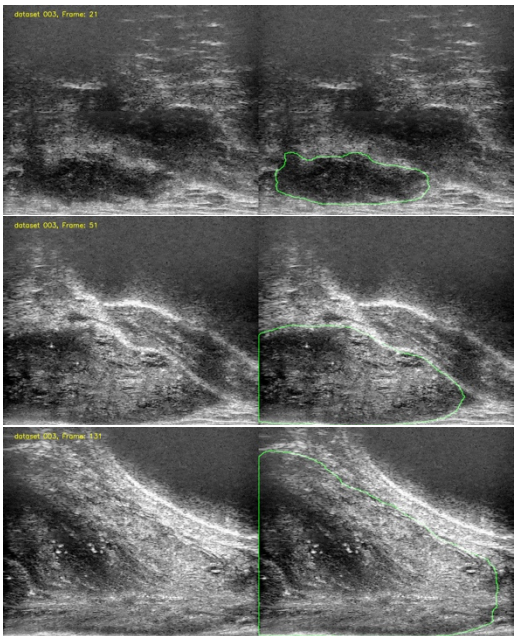

Fig. 8. Example of segmentation results overlayed on top of the raw micro-ultrasound images for qualitative assessment.

5. CONCLUSION

In this study, we developed a modified UNet deep neural network model and trained it with Micro-Ultrasound images from a pilot dataset, achieving satisfactory performance. Our preliminary results demonstrated high accuracy in prostate segmentation of the prostate capsule and assessed with 10-fold cross-validation. Furthermore, the qualitative results demonstrated that automated annotation of the prostate capsule could be performed in Micro-Ultrasound images and could assist prostate cancer surgeons during the in-bore biopsy. Real-time prostate annotation may optimize surgeons' time and improve precision. In the future, this can significantly impact the active surveillance monitoring and treatment planning for prostate cancer patients.

One of the limitations of this pilot study was the small number of subjects. In our future work we plan to perform a larger scale study and test the method across a wider pool of subjects, which could improve the robustness of the training and avoid potential overfitting problems. Finally, we plan to extend our method to perform segmentation of other anatomical structures within the capsule, which will be the subject of our future studies.

6. ACKNOWLEDGMENTS

This project was supported by a grant form the Prostate Cancer Foundation. The authors acknowledge the University of Florida Research Computing and the Digital Worlds Institute for providing computational resources and support that have contributed to the research results reported in this publication.

7. REFERENCES

[1] R. L. Siegel, K. D. Miller, H. E. Fuchs, and A. Jemal, "Cancer statistics, 2022.," *CA. Cancer J. Clin.*, vol. 72, no. 1, pp. 7–33, Jan. 2022, doi: 10.3322/caac.21708.

[2] M. Borghesi *et al.*, "Complications After Systematic, Random, and Image-guided Prostate Biopsy.," *Eur. Urol.*, vol. 71, no. 3, pp. 353–365, Mar. 2017, doi: 10.1016/j.eururo.2016.08.004.

[3] H. U. Ahmed *et al.*, "Diagnostic accuracy of multi-parametric MRI and TRUS biopsy in prostate cancer (PROMIS): a paired validating confirmatory study.," *Lancet (London, England)*, vol. 389, no. 10071, pp. 815–822, Feb. 2017, doi: 10.1016/S0140-6736(16)32401-1.

[4] V. Kasivisvanathan *et al.*, "MRI-Targeted or Standard Biopsy for Prostate-Cancer Diagnosis.," *N. Engl. J. Med.*, vol. 378, no. 19, pp. 1767–1777, May 2018, doi: 10.1056/NEJMoa1801993.

[5] P. Sountoulides *et al.*, "Micro-Ultrasound-Guided vs Multiparametric Magnetic Resonance Imaging-Targeted Biopsy in the Detection of Prostate Cancer: A Systematic Review and Meta-Analysis.," *J. Urol.*, vol. 205, no. 5, pp. 1254–1262, May 2021, doi: 10.1097/JU.0000000000001639.

[6] S. Ghai *et al.*, "Assessing cancer risk on novel 29 MHz micro-ultrasound images of the prostate: creation of the micro-ultrasound protocol for prostate risk identification," *J. Urol.*, vol. 196, no. 2, pp. 562–569, 2016, doi: 10.1016/j.juro.2015.12.093.

[7] G. Eure, D. Fanney, J. Lin, B. Wodlinger, and S. Ghai, "Comparison of conventional transrectal ultrasound, magnetic resonance imaging, and micro-ultrasound for visualizing prostate cancer in an active surveillance population: A feasibility study," *Can. Urol. Assoc. J.*, vol. 13, no. 3, pp. E70–E77, 2019, doi: 10.5489/cuaj.5361.

[8] F. Pollastri, M. Cipriano, F. Bolelli, and C. Grana, "LONG-RANGE 3D SELF-ATTENTION FOR MRI PROSTATE SEGMENTATION Department of Engineering ' Enzo Ferrari ,' University of Modena and Reggio Emilia , Modena , Italy," *2022 IEEE 19th Int. Symp. Biomed. Imaging*, 2022.

[9] H. Wang *et al.*, "A Feature Regularization Based Meta-Learning Framework for Generalizing Prostate Mri Segmentation," in *2022 IEEE 19th International Symposium on Biomedical Imaging (ISBI)*, 2022, pp. 1–4, doi: 10.1109/ISBI52829.2022.9761564.

[10] Y. Lei *et al.*, "Ultrasound prostate segmentation based on multidirectional deeply supervised V-Net," *Med. Phys.*, vol. 46, no. 7, pp. 3194–3206, 2019, doi: 10.1002/mp.13577.

[11] S. Vesal *et al.*, "Domain generalization for prostate segmentation in transrectal ultrasound images: A multi-center study," *Med. Image Anal.*, vol. 82, no. September, p. 102620, 2022, doi: 10.1016/j.media.2022.102620.

[12] N. Orlando, D. J. Gillies, I. Gyacskov, C. Romagnoli, D. D'Souza, and A. Fenster, "Automatic prostate segmentation using deep learning on clinically diverse 3D transrectal ultrasound images," *Med. Phys.*, vol. 47, no. 6, pp. 2413–2426, 2020, doi: 10.1002/mp.14134.

[13] C. M. Laurence Klotz, "Can high resolution micro-ultrasound replace MRI in the diagnosis of prostate cancer?," *Eur. Urol. Focus*, vol. 6, no. 2, pp. 419–423, Mar. 2020, doi: 10.1016/j.euf.2019.11.006.

[14] O. Ronneberger, P. Fischer, and T. Brox, "U-Net: Convolutional Networks for Biomedical Image Segmentation BT - Medical Image Computing and Computer-Assisted Intervention – MICCAI 2015," 2015, pp. 234–241.

[15] C. Huang *et al.*, "Applying deep learning in recognizing the femoral nerve block region on ultrasound images," *Ann. Transl. Med.*, vol. 7, no. 18, pp. 453–453, 2019, doi: 10.21037/atm.2019.08.61.